SURFACE DEFINITION AND GRID GENERATION ABOUT A CREW EMERGENCY RESCUE VEHICLE (CERV) FOR SPACE STATION FREEDOM

Robert E. Smith and Eric L. Everton
Analysis and Computation Division
NASA Langley Research Center
Hampton, Virginia 23665

Michael R. Wiese and Norma Farr
Computer Sciences Corporation
Hampton, Virginia 23665

Introduction

All Computational Fluid Dynamics simulations require the generation of a grid that covers the flow-field domain and its boundaries. In order to obtain an accurate solution, the grid must be concentrated in regions where there are large gradients, and the grid must possess favorable mathematical characteristics, such as acceptable grid skewness.

For the flow about an aerospace vehicle, such as the Crew Emergency Rescue Vehicle (CERV), a grid on the configuration boundary surface must be created and integrated into an overall grid. The vehicle surface grid is extracted from a **numerical model** obtained from either a Computer-Aided Design system (**CAD**)or from measurement of a physical model.

The numerical model of the CERV vehicle is obtained from the measurement of a 5.9 inch long wind-tunnel model. This measuring instrument obtains two coordinates around the model at fixed stations in the third coordinate. Defining the vehicle geometry in a right-hand Cartesian coordinate system, the origin of the coordinate system is at the most forward point of the vehicle. The negative z-axis extends down the vehicle, the y-axis is in the span-wise direction, and the x-axis is in the vertical direction . The measured data base consists of x, y surface coordinates at twenty z stations (cross sections)

down the vehicle.

Measured coordinates have associated measurement errors, and there is the possibility of roughness on the model itself which could occur in the manufacturing process. An interrogation of the plotted cross sections of the CERV model reveals a number of serious irregularities which could be due to measurement error or surface roughness. If the irregularities are allowed in the computational grid, they will ultimately appear in the numerical solution, and therefore, require a statistical evaluation. Alternately, the numerical model can be initially idealized by smoothing the measured data. Also, there may be surface characteristics that are not included in a CFD solution.

Surface Smoothing

To remove imperfections in the measured data, a cubic spline smoothing algorithm [1] is applied to the coordinates at each z cross section. The application of the algorithm starts with the creation of a parametric independent variable t, which is the approximated arc length along a cross section. The x and y coordinates are considered to be functions $x(t)$ and $y(t)$. The functions are determined from the sets of parametric data

$$\{x_i, t_i\}_{i=1}^{i=n} \qquad \{y_i, t_i\}_{i=1}^{i=n}$$

where x_i and y_i are the ith measured coordinates on a cross section, t_i is the approximate arc length at the ith point and n is the number of measured points on a cross section and varies from cross section to cross section. The approximate arc length is defined by

$$t_{i+1} = \sqrt{(x_{i+1} - x_i)^2 + (y_{i+1} - y_i)^2} + t_i$$

where $t_1 = 0$. This computation starts on the bottom of the vehicle at the symmetry plane and continues around to the top of the vehicle at the symmetry plane. After the maximum approximate arc length is computed, the variable t is redefined to be the normalized approximate arc length by

$$t_i = \frac{t_i}{t_n}$$

The functions $x(t)$ and $y(t)$ are represented in vector form

$$\mathbf{X}(t) = \left\{ \begin{array}{c} x(t) \\ y(t) \end{array} \right\}$$

and the cubic spline representation is

$$\mathbf{X}(t) = \left\{ \mathbf{A}_i + \mathbf{B}_i(t - t_i) + \mathbf{C}_i(t - t_i)^2 + \mathbf{D}_i(t - t_i)^3 \right\}_{i=1}^{i=n-1} \tag{1}$$

where

$$\mathbf{A}_i = \left\{ \begin{array}{c} a_{x_i} \\ a_{y_i} \end{array} \right\} \mathbf{B}_i = \left\{ \begin{array}{c} b_{x_i} \\ b_{y_i} \end{array} \right\} \mathbf{C}_i = \left\{ \begin{array}{c} c_{x_i} \\ c_{y_i} \end{array} \right\} \mathbf{D}_i = \left\{ \begin{array}{c} d_{x_i} \\ d_{y_i} \end{array} \right\}$$

The spline conditions are

$$\left. \begin{array}{l} \mathbf{X}_i(t_{i+1}) = \mathbf{X}_{i+1}(t_{i+1}) \\ \frac{d\mathbf{X}_i}{dt}(t_{i+1}) = \frac{d\mathbf{X}_{i+1}}{dt}(t_{i+1}) \\ \frac{d^2\mathbf{X}_i}{dt^2}(t_{i+1}) = \frac{d^2\mathbf{X}_{i+1}}{dt^2}(t_{i+1}) \end{array} \right\} (i = 1, 2 \cdots n-2, 0 \leq t \leq t_n)$$

The coefficients $\{\mathbf{A}_i, \mathbf{B}_i, \mathbf{C}_i, \mathbf{D}_i\}_{i=1}^{i=n-1}$ are undetermined parameters whose solution define $\mathbf{X}(t)$ in Equation (1). The objective is to find the coefficients which minimize the integral of second derivatives squared

$$\int_0^{t_n} [\mathbf{X}''(t)]^2 \, dt$$

subject to the constraint

$$\sum_{i=1}^{n} \left[\frac{\mathbf{X}(t_i) - \mathbf{X}_m(t_i)}{\delta \mathbf{X}_i} \right]^2 \leq E$$

where

$$\mathbf{X}_m(t_i) = \left\{ \begin{array}{c} x_i \\ y_i \end{array} \right\} \qquad \delta\mathbf{X}_i = \left\{ \begin{array}{c} \delta x_i \\ \delta y_i \end{array} \right\}$$

and E is a positive constant specifying the extent of smoothing. The vector $\delta\mathbf{X}$ is the allowable deviation of the spline function $\mathbf{X}(t)$ and the measured surface coordinates $\mathbf{X}_m$. The restated objective is to find the smoothest cubic spline passing within the bounds

$$\mathbf{X}_m(t_i) - \delta\mathbf{X}_i \leq \mathbf{X}_m(t_i) \leq \mathbf{X}_m(t_i) + \delta\mathbf{X}_i$$

where $\delta\mathbf{X}_i$ is the maximum deviation of the spline functions from the measured coordinates.

The method of Lagrange multipliers from the calculus of variations is used to find the parameters

$$\mathbf{S}_k = \{\mathbf{A}_i, \mathbf{B}_i, \mathbf{C}_i, \mathbf{D}_i\}_{i=1}^{i=n_k-1}$$

where the index k denotes the kth cross section in the stream-wise direction. The solution algorithm for spline smoothing can be found in reference 1. The technique exists in subroutine form on the Langley math library (SUBROUTINE CSDSES)[2]. A main program is written to read the measured coordinates, compute the approximate arc length and call the spline smoothing subroutine for each coordinate. It is necessary to provide the allowable derivations $\{\delta\mathbf{X}_i\}_{i=1}^{i=n_k}$, and the constant E is set equal $n_k - 1$. Figures 1 shows the application of the smoothing procedure to one of the cross sections from the CERV vehicle.

Surface Grid

The technique described above smooths the measured data at each cross section in only one direction. The next step is to distribute points along the smoothed cross sections in the fashion that is desired for the final grid points. These points are then smoothed and interpolated in the stream-wise direction for the surface grid points. The initial desired distribution of points on the CERV vehicle is uniform around the vehicle near the front and concentrated at the wingtip as the wing emerges from the fuselage down stream. The streamwise distribution should be concentrated near the front of the vehicle.

If N is the number of grid points around the body and the index I denotes the Ith grid point, a computational coordinate ξ around the body is defined by

$$\xi = (I-1)/(N-1)$$

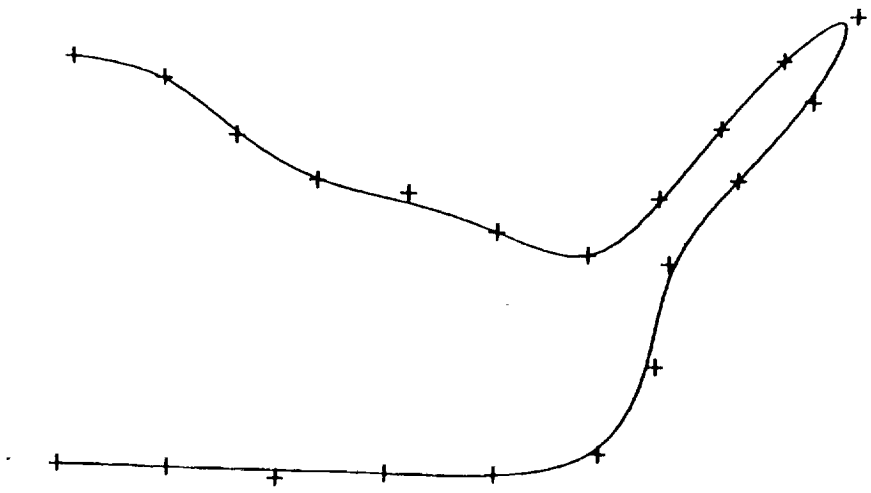

Figure 1: Spline Smoothing

and ξ is mapped into the normalized approximate arc length t with the variable $\bar{t}$. Interpolated $\bar{x}$ and $\bar{y}$ coordinates are obtained from $\mathbf{S}_k$ and Equation 1 given $\bar{t}$.

In the streamwise direction and up to the wing root, the desired grid spacing is uniform and $\bar{t} = \xi$. At the wing root the distribution becomes a bi-exponential defined by

$$\bar{t} = t_e \frac{e^{\Gamma_1 \xi} - 1}{e^{\Gamma_1} - 1}$$

$$0 \leq \xi \leq \xi_e \qquad 0 \leq \bar{t} \leq t_e$$

$$\bar{t} = t_e + (1 - t_e) \frac{e^{\Gamma_2 \frac{\xi - \xi_e}{1 - \xi_e}} - 1}{e^{\Gamma_2} - 1}$$

$$\xi_e \leq \xi \leq 1 \qquad t_e \leq \bar{t} \leq 1$$

where ξ_e is the desired percentage of grid points around the bottom of the vehicle up to the wing leading edge, and t_e is the normalized approximate arc length along the same curve up the wing leading edge. The constant Γ_1 governs the amount of concentration at the wing tip, and Γ_2 is computed using a Newton-Raphson iteration to assure continuity of $\frac{Dt}{D\xi}(\xi_e)$. The parameters, ξ_e, t_e and Γ_1 vary in the streamwise direction from the wing root to the end of the wing.

The computation of the surface grid is based on smoothing the previously- defined data in the streamwise direction. The parametric form of the smoothed cross section data in the streamwise direction is

$$\{\bar{x}_{I,k}, s_k\}_{I=1,k=1}^{I=N,k=m} \qquad \{\bar{y}_{I,k}, s_k\}_{I=1,k=1}^{I=N,k=m} \qquad \{z_k, s_k\}_{k=1}^{k=m}$$

where z_k is the negative z-coordinate of the kth cross section, m is the number of cross sections, and s is the normalized approximate arc length in the streamwise direction defined by

$$s_{I,k+1} = \sqrt{(\bar{x}_{I,k+1} - \bar{x}_{I,k})^2 + (\bar{y}_{I,k+1} - \bar{y}_{I,k})^2 + (z_{k+1} - z_k)^2} + s_k$$

$$s_{I,1} = 0$$

The computation of $s_{I,k}$ starts at the nose of the vehicle and ends at $k = m$. Again, after the maximum approximate arc length is computed for each I, s is normalized with respect to the maximum value. The same procedure that was used to represent a cubic spline approximation for $\mathbf{X}(t)$ is used to compute $\mathbf{X}(I, s)$ where

$$\mathbf{X}(I,s) = \left\{ \begin{array}{c} x(I,s) \\ y(I,s) \\ z(I,s) \end{array} \right\}$$

and the cubic spline representation is

$$\mathbf{X}(I,s) = \left\{ \bar{\mathbf{A}}_{I,k} + \bar{\mathbf{B}}_{I,k}(s - s_k) + \bar{\mathbf{C}}_{I,k}(s - s_k)^2 + \bar{\mathbf{D}}_{I,k}(s - s_k)^3 \right\}_{I=1,k=1}^{I=N,k=m} \tag{2}$$

where

$$\bar{\mathbf{A}}_{I,k} = \left\{ \begin{array}{c} a_{x_{I,k}} \\ a_{y_{I,k}} \\ a_{z_{I,k}} \end{array} \right\} \bar{\mathbf{B}}_{I,k} = \left\{ \begin{array}{c} b_{x_{I,k}} \\ b_{y_{I,k}} \\ b_{x_{I,k}} \end{array} \right\} \bar{\mathbf{C}}_{I,k} = \left\{ \begin{array}{c} c_{x_{I,k}} \\ c_{y_{I,k}} \\ c_{x_{I,k}} \end{array} \right\} \bar{\mathbf{D}}_{I,k} = \left\{ \begin{array}{c} d_{x_{I,k}} \\ d_{y_{I,k}} \\ d_{x_{I,k}} \end{array} \right\}$$

The procedure described above is used to compute $\bar{S}_I = \left\{ \bar{\mathbf{A}}_{I,k}, \bar{\mathbf{B}}_{I,k}, \bar{\mathbf{C}}_{I,k}, \bar{\mathbf{D}}_{I,k} \right\}_{I=1,k=1}^{I=N,k=m}$ where

$$\delta \mathbf{X}_{I,k} = \left\{ \begin{array}{c} \delta \bar{x}_{I,k} \\ \delta \bar{y}_{I,k} \\ 0 \end{array} \right\}$$

If M is the number of grid points along the body in the streamwise direction, and the index K denotes the Kth grid point, a computational coordinate ζ along the vehicle is defined by

$$\zeta = \frac{(K-1)}{(M-1)}$$

and ζ is mapped into the normalized approximate arc length s. A concentration of grid points near the front of the vehicle is achieved by using the transformation

$$\bar{s} = \frac{e^{\Gamma_3 \zeta} - 1}{e^{\Gamma_3} - 1}$$

The constant Γ_3 determines the amount of concentration. A surface grid $\{X(I,K), Y(I,K), Z(I,K)\}_{I=1,K=1}^{I=N,K=M}$ is obtained by evaluation with Equation 2 given $\bar{s}$.

Starting with the measured data, a surface grid for the CERV vehicle, where $N = 81$ and $M = 125$, is shown in Figure 2. This boundary surface grid is then used in the computation of the volume grid about the vehicle.
The volume grid is designed to capture all of the shock phenomena and provide for reasonable estimates of heating on the lower surface of the vehicle for high Mach numbers and high angles of attack.

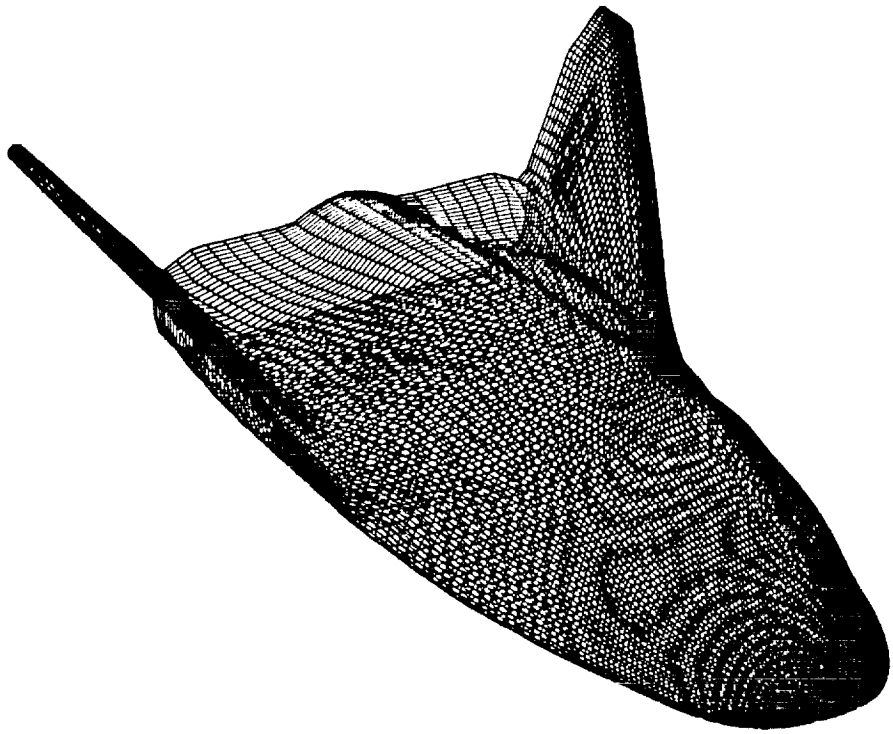

Figure 2: CERV Surface Grid

The grid topology chosen for the CERV flow field is a **dual-block** topology similar to that described in reference 3. In this topology, there is an inner block beginning from a singularity line just upstream of the wing root. A second block surrounds the forward part of the vehicle and the inner block. In reference 3, the lifting surfaces on the configuration has sharp leading edges, whereas, the CERV wing has a rounded leading edge. Consequently, the outer boundary surface of the inner-grid block is displaced forward of the wing leading edge so that a C-type grid is formed spanwise about the wing.

The advantage of using a two-block topology compared to a single-block topology is that the flow field region can be adequately covered with fewer points. That is, in order to have enough points to cover the region between the wing and symmetry plane, a single block would require many more points in the forward region than is necessary. The disadvantages are the additional program complexity in the solution code and the numerical complications at the singularity line.

Inner-Block Volume Grid

The inner block is bounded by the vehicle surface, the outer boundary sur-

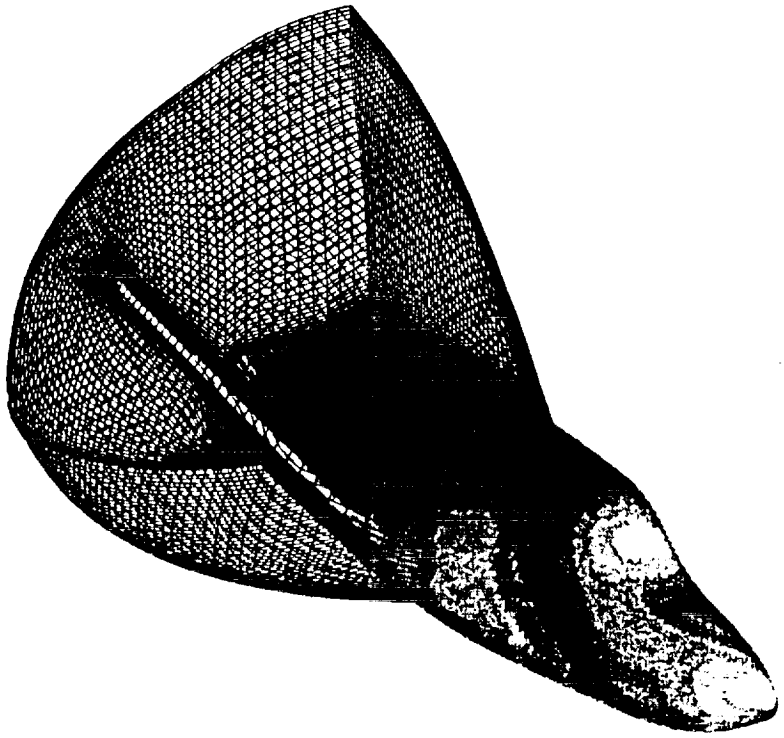

Figure 3: Inner-Block Grid

face of the inner block, the bottom-symmetry surface, the top-symmetry surface, the singularity line and the downstream surface (Fig. 3). The outer boundary surface is defined by creating an analytical curve, translating the curve to the singularity line and rotating it around the vehicle stretching in the spanwise direction and skewing it upward as it passes over the top of the vehicle. This is very similar to the surface boundary generation that is described in reference 3 with the addition of the stretching and skewing. The interior grid and the distribution of grid points on the outer-boundary surface, symmetry-plane surfaces and the downstream surface are computed using a three-dimensional version of the Two-Boundary Grid Generation technique (TBGG) described in reference 4. The grid points are concentrated at the vehicle surface and near orthogonality is maintained. Figure 4 shows the inner grid on the downstream boundary surface. As the singularity line is approached from downstream, the distribution approaches a uniform distribution matching the distribution upstream of the singularity line.

Outer-Block Volume Grid

The grid on the outer block surrounds the forward part of the fuselage and the grid on the inner block. The six surfaces forming the outer block are:

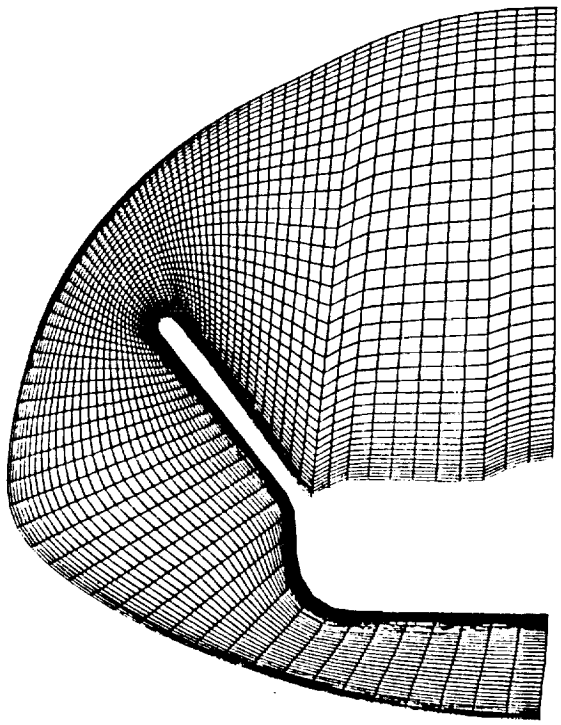

Figure 4: Downstream Surface Grid Inner Block

(1) the forward fuselage and outer boundary surface on the inner block; (2) a far-field boundary surface; (3) the symmetry plane on the bottom side of the vehicle; (4)the symmetry plane on the top side of the vehicle; (5) a polar singularity line extending from the $(0, 0, 0)$ point of the vehicle to the far-field boundary surface; and (6) a downstream surface extending the inner block to the far-field boundary.

The first computation for the outer block is the far-field boundary surface which is similar to computing the outer boundary surface for the inner-grid block. The characteristics of the far-field boundary are that it is relatively close to the vehicle on the bottom side and relatively far away on the top side to be just outside of the bow shock. Further, it should expand away from the wings in the spanwise direction to capture the shock phenomenon.

Instead of using a single analytical curve and rotating it around the vehicle, two curves are blended in the streamwise direction to create another curve that is translated to a point about four shock stand-off distances from the nose, and rotated about the vehicle while being stretched in the spanwise and vertical directions. The two blended curves are chosen such that one is suitable forward and the other is suitable rearward. Grid points are dis-

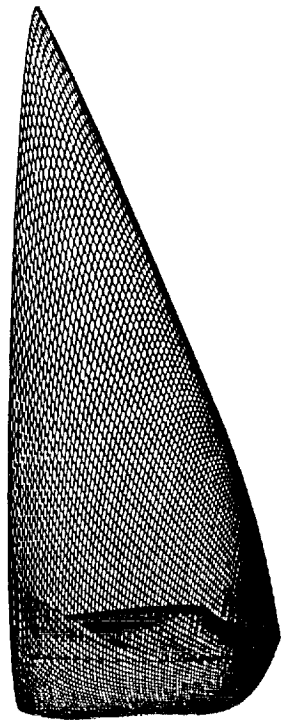

Figure 5: Far-Field Boundary Surface/Grid

tributed rearward and around the outer boundary approximately across from the corresponding points on the opposite-side surface. A side view of the far field surface is shown in Figure 5.

The general approach for computing the outer-block grid is transfinite interpolation [5], given grid point information at block boundaries and intermediate surfaces. The outer block computation is divided into two parts: (1) the forward part from the nose singularity line back to a surface extending from the singularity line around the fuselage to the far field boundary (singularity-line surface); and (2) a rearward part extending from the singularity-line surface to the downstream surface.

The forward part of the outer block is obtained by first computing grid points on the bottom symmetry plane, top symmetry plane and a spanwise surface nearly orthogonal to the symmetry plane. The TBGG algorithm is applied in order to concentrate grid points near the vehicle surface and maintain near orthogonality. Figure 6 shows the three surfaces. Transfinite interpolation with linear/exponential blending functions is used to fill in the interior.

The rearward part on the outer block is computed using transfinite inter-

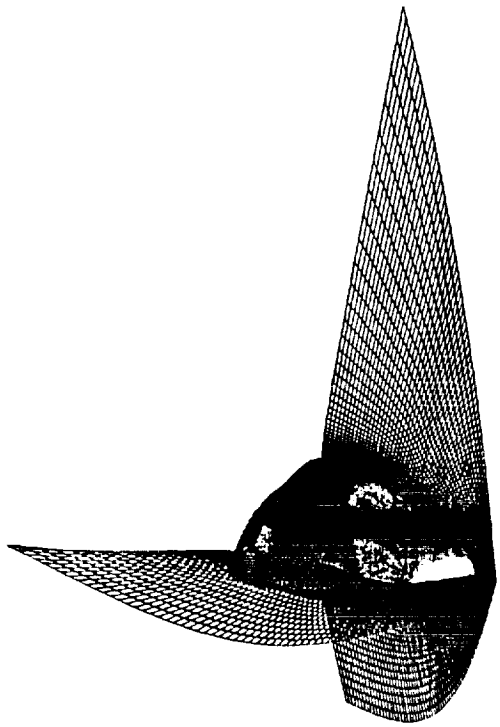

Figure 6: Surface Grids Used For Volume Grid Computation

polation with Lagrangian blending functions [6]. This allows first derivative continuity in grid spacing and grid curve direction except in the neighborhood of the singularity line. A concentration of grid points in this region is used to overcome this deficiency. Figure 7 shows grid points in the symmetry plane and two spanwise surfaces in the streamwise direction. The final paper will present more details on how the allowable derivations $\delta \mathbf{X}$ between the measured and computed surface coordinates are obtained. Also, there will be more detail on the interactive software to compute the volume grid.

REFERENCES

1. Reinsch, C. H.: Smoothing by Spline Functions, *Numer. Math.,* vol 10, no 3 1967, pp177-183.

2. Anonymous: Mathematical and Statistical Software at Langley, E3.3, Document N2-33, March, 1988.,

3. Smith, R. E. and Everton, E. L.: Interactive Grid Generation For Fighter Aircraft Geometries, *Numerical Grid Generation in Computational Fluid Mechanics '88*, Pineridge Press, 1988, pp 805-814.

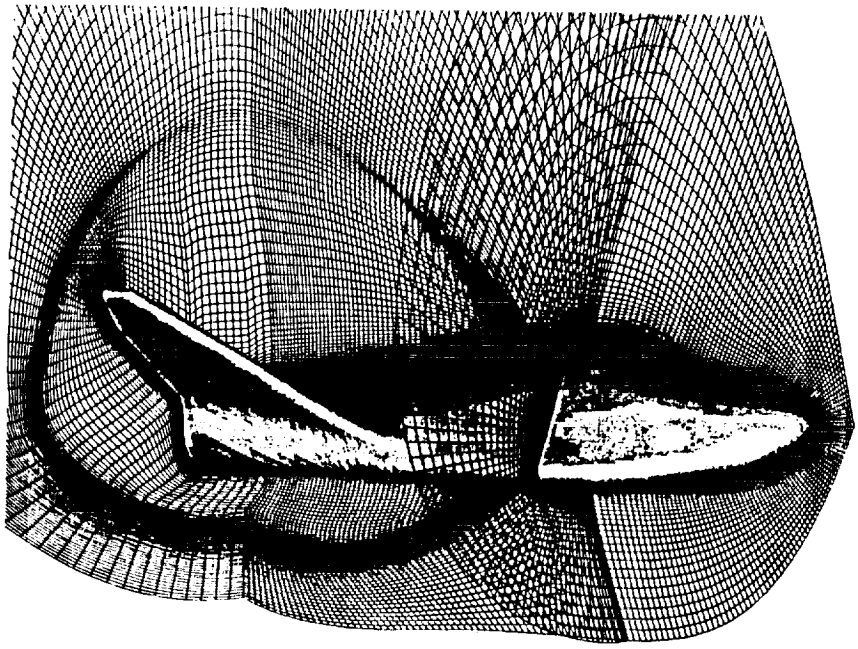

Figure 7: Volume Grid About The CERV Vehicle

4. Smith, R. E. and Wiese, M. R.: Interactive Grid Generation Technique, NASA TP 2533, 1986.

5. Smith, R. E. and Eriksson, L.-E.: Algebraic Grid Generation, *Comput. Meths. Appl. Mech. Engrg.* 64, pp 285-300, 1987.

6. Eriksson, L-E, Smith, R. E., Wiese, M. R., and Farr, N.: Grid Generation and Inviscid Flow Computation About a Cranked- Winged Airplane Geometry. *Jou. of Aircraft*, Vol.25, No. 9 1988, pp 820-826.

LIST OF FIGURES

Fig. 5-Far-Field Boundary Surface/Grid.

Fig. 6-Surface Grids Used for Volume Grid Computation.

Fig. 7-Volume Grid About CERV Vehicle.